8-2021

# Study of Nonlinear Optical Properties of Gold Nanoparticles Dispersed in Nematic Liquid Crystals

Changshuo Fu

# STUDY OF NONLINEAR OPTICAL PROPERTIES OF GOLD NANOPARTICLES DISPERSED IN NEMATIC LIQUID CRYSTALS

A Thesis Presented

by

CHANGSHUO FU

Submitted to the Office of Graduate Studies,
University of Massachusetts Boston,
in partial fulfillment of the requirements for the degree of

MASTER OF SCIENCE

August 2021

Applied Physics Program

STUDY OF NONLINEAR OPTICAL PROPERTIES OF GOLD NANOPARTICLES DISPERSED IN NEMATIC LIQUID CRYSTALS

A Thesis Presented

by

CHANGSHUO FU

Approved as to style and content by:

_____
Chandra Yelleswarapu, Associate Professor
Chairperson of the Committee

_____
Mohamed Amine Gharbi, Assistant Professor
Member

_____
Jonathan Celli, Associate Professor
Member

_____
Jonathan Celli, Program Director
Applied Physics Program

_____
Rahul Kulkarni, Chair
Physics Department

ABSTRACT

STUDY OF NONLINEAR OPTICAL PROPERTIES OF GOLD NANOPARTICLES DISPERSED IN NEMATIC LIQUID CRYSTALS

August 2021

Changshuo Fu

B. S. Boston University
M. S. University of Massachusetts Boston

Directed by Professor Chandra Yelleswarapu

Gold nanoparticles come in various sizes and shapes. Their optical properties arise from surface plasmon resonance, collective excitation/oscillation of conduction electrons. The study of the nonlinear optical properties of these materials is essential for photonic and biomedical applications. In this thesis, nonlinear optical properties of gold nanoparticles dispersed in the nematic liquid crystal were studied using optical and photoacoustic Z-scan techniques. Results show enhanced nonlinearity when gold is dispersed in planar-oriented 5CB liquid crystals compared to when liquid crystals were not oriented (degenerate). Also, sample with low gold concentration, by weight percentage, shows the better nonlinearity. Reasons behind the influence of the nonlinear effect and future plans were also discussed.

# ACKNOWLEDGMENTS

In the end, I am truly grateful to Professor Chandra Yelleswarapu, my graduate research advisor, for his kind guidance and help. It is my pleasure to work as a graduate student with him. I sincerely thank all the help I get from him and all the guidance he provides me, not only in the research aspect but also in my life and further academic study. I am also thankful for the help and suggestion from Shengwei Wang, who works together with me in the lab. Additionally, I appreciate Professor Mohamed Amine Gharbi, for the help and guidance in the Liquid crystal field and for recommending me to Professor Chandra.

I want to say Thank you to my thesis committee members: Professor Chandra Yelleswarapu, Professor Mohamed Amine Gharbi, and Professor Jonathan Celli. Again, I truly appreciate the time and the effort they have put into my thesis.

Most importantly, I want to say thank you to my parents and all my family members. The achievements I got so far would not have been possible without their love and support.

TABLE OF CONTENTS

ABSTRACT iv

ACKNOWLEDGMENTS v

LIST OF FIGURES viii

LIST OF TABLES ix

CHAPTER Page

PART I. INTRODUCTION

1.1 Nonlinear optics 1
1.2 Photoacoustic effect 2
1.2.1 Background and introduction 2
1.2.2 Photoacoustic applications 3
1.3 Surface Plasmon Resonance (SPR) 4
1.3.1 Surface plasmon resonance in gold nanoparticles 5
1.4 Optical Z-scan technique 6
1.5 Nonlinear optical absorption properties 8
1.5.1 Nonlinear absorption 8
1.5.2 Open aperture Z-scan nonlinearities 10
1.5.3 Photoacoustic Z-scan 11
1.6 Liquid crystal 12
1.6.1 Nematic liquid crystal 12
1.6.2 SPR of gold nanoparticles in nematic liquid crystals 13

PART II. EXPERIMENT SETUP

2.1 Materials 15
2.2 Sample preparation 16
2.3 Polarizing microscope 18
2.4 UV-Vis Optical absorption Spectrum 19
2.5 Photoacoustic Z-scan setup 19

CHAPTER Page

PART III. RESULT & DISCUSSION

3.1 Image using polarizing microscope 22
3.1.1 Liquid crystals vs water as medium 22
3.1.2 Planar-oriented Vs. Planar-degenerated 23
3.2 Absorbance and absorption coefficient 26
3.3 Photoacoustic and optical signal 28
3.3.1 Photoacoustic/optical signal and nonlinear coefficient β under 10Hz 29
3.3.2 Photoacoustic/optical signal and nonlinear coefficient β under 5Hz 32
3.3.3 Photoacoustic/optical signal and nonlinear coefficient β under 2Hz 34
3.4 Planar-oriented sample Vs. Planar-degenerated sample 36

PART IV. CONCLUSION & FURTHER STUDY

4. Conclusion and further study 38

REFERENCE 39

LIST OF FIGURES

FIGURE Page

Figure 1 The schematic of photoacoustic effect 3

Figure 2 Schematic of the creation of surface plasmon resonance in Au nanoparticles 6

Figure 3 The schematic of the Z-scan technique 8

Figure 4 The schematic of linear/nonlinear absorption 8

Figure 5 Energy level models of SA and RSA 9

Figure 6 The schematic of Nematic liquid crystal molecule's orientation 12

Figure 7 SPR of gold nanoparticles in Panar-degenerated/Planar-oriented samples 14

Figure 8 Materials used 15

Figure 9 Samples of pure gold nanoparticles solution cells 17

Figure 10 Samples of gold nanoparticles dispersed in nematic liquid crystals 17

Figure 11 The schematic of Polarizing microscope 18

Figure 12 Cary 60 UV-Vis 19

Figure 13 Real PAZ-scan setup 21

Figure 14 Interface of LabView 21

Figure 15 Sample of gold nanoparticles dispersed in water and with liquid crystals 23

Figure 16 Samples under cross polarizer: planar-oriented and planar-degenerated 25

Figure 17 UV-Vis spectrum for all samples 27

Figure 18 Curve fitting and PA/OPT signal under 10 Hz 31

Figure 19 Curve fitting and PA/OPT signal under 5 Hz 33

Figure 20 Curve fitting and PA/OPT signal under 2 Hz 35

Figure 21 Planar-oriented sample Vs. Planar-degenerated sample 37

LIST OF TABLES

TABLE Page

Table 1 Information of materials 15

Table 2 Absorbance and linear absorption of all samples 28

Table 3 Values of nonlinear coefficient of different samples under 10Hz 31

Table 4 Values of nonlinear coefficient of different samples under 5Hz 33

Table 5 Values of nonlinear coefficient of different samples under 2Hz 35

Table 6 Values of nonlinear coefficient of samples 37

CHAPTER 1

# 1. INTRODUCTION

## 1.1 Nonlinear optics

The optical properties of materials are modified by high-intensity light such as a laser. The study of this phenomenon is called Nonlinear Optics. This phenomenon is observed in a wide variety of materials like dyes, polymers, semiconductors, nanomaterials, Etc. After the invention of the first work laser by Theodore Maiman in 1960, Peter Franken et al demonstrated the first nonlinear optical phenomenon – second-harmonic generation – in 1961. This has been considered the beginning of the study of nonlinear optics [1].

To have a comprehensive understanding of optical nonlinearity, consider the measurement of the electrical polarity of a system of charges, also known as polarization $\vec{P}(t)$. $\vec{P}(t)$ of the material is related to the intensity of the applied optical field E(t). In the cases where the material's response is linear to the applied optical field, the polarization $\vec{P}(t)$ is linearly dependent on the intensity of the electric field $\vec{E}(t)$:

$$\vec{P}(t) = \varepsilon_0 \chi^{(1)} \cdot \vec{E}(t) \tag{1.1.1}$$

where $\chi^{(1)}$ represents the linear optics and $\varepsilon_0$ is the permittivity of free space.

When we consider the case of nonlinear optics, we can describe the response of the optical system by expressing the polarization $\vec{P}(t)$ as a power series that depends on the intensity of the electric field $\vec{E}(t)$. The relationship can be described by the following equation:

$$\vec{P}(t) = \epsilon_0 \{ \chi^{(1)} \cdot \vec{E}(t) + \boldsymbol{\chi}^{(2)} \cdot \vec{E}^{\mathbf{2}}(\boldsymbol{t}) + \boldsymbol{\chi}^{(3)} \cdot \vec{E}^{\mathbf{3}}(\boldsymbol{t}) + \ldots\ldots \}$$

$$= \vec{P}^{(\mathbf{1})}(\boldsymbol{t}) + \vec{P}^{(\mathbf{2})}(\boldsymbol{t}) + \vec{P}^{(\mathbf{3})}(\boldsymbol{t}) + \ldots\ldots \quad (1.1.2)$$

where $\vec{P}(t)$ is polarization, $\vec{E}(t)$ is applied electric field; the second-order and third-order nonlinear optical susceptibilities are described as $\chi^2$ and $\chi^3$. The third-order nonlinear susceptibility is a complex quantity. The real and imaginary parts describe nonlinear refraction (NLR) and nonlinear absorption (NLA) or gain. The third-order nonlinear susceptibility can be expressed as a complex quantity:

$$\chi^{(3)} = \chi_{\mathrm{R}}^{(3)} + \mathrm{i}\chi_{\mathrm{I}}^{(3)} \quad (1.1.3)$$

with

$$\chi_{\mathrm{R}}^{(3)} = 2\mathrm{n}_0^2\varepsilon_0 \mathrm{c}\gamma \quad (1.1.4)$$

and

$$\chi_{\mathrm{I}}^{(3)} = \frac{\mathrm{n}_0\varepsilon_0\mathrm{c}^2\beta}{\omega} \quad (1.1.5)$$

Where $n_0$ is the linear refractive index, $\varepsilon_0$ is the permittivity in a vacuum, $I_0$ is the irradiance of the laser beam within the sample, c is the speed of light in the free space, and $\omega$ is the optical frequency. Optical materials with high third-order nonlinear optical coefficients are much needed for photonic and biomedical applications. In this regard, for the past few decades, extensive research efforts have been dedicated to developing novel and high-performance nonlinear optical (NLO) materials [2].

## 1.2 Photoacoustic effect

### 1.2.1 Background and introduction

The photoacoustic effect is a physical phenomenon that was discovered by Alexander G. Bell in 1880. He initially wanted to invent a communication device that is pretty like the cell phone in the modern world [3].

When light is absorbed by a material, the material undergoes thermo-elastic expansion, which in turn generates pressure waves in the material [4] [5]. The creation of the pressure wave because of photon absorption is known as the photoacoustic effect, and the propagating wave is called the photoacoustic wave. These ultrasonic waves can be detected by the ultrasonic sensor, as shown in Figure 1.

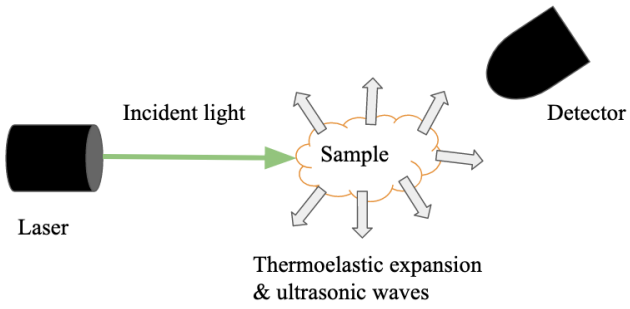


Figure 1: The schematic of the photoacoustic effect

### 1.2.2 Photoacoustic applications

The photoacoustic (PA) effect has recently found applications in various fields such as biomedical imaging, therapeutics, and bioengineering. In biomedical imaging, the energy from light or laser is absorbed by chromophores which will cause a photoacoustic effect in organs and tissues. The waves or signals generated by the PA effects in the deep tissues can be detected by the ultrasound sensors that are placed at the surface. Photoacoustic imaging (PAI) is a safe and

non-invasive technique that combines the characteristics of ultrasound imaging, high resolution, and the properties of optical imaging, high contrast. First proposed in the 1990s [6.7], the photoacoustic medical imaging was tested and applied to live animals in nine years, 1999 [8]. The contrast of PAI depends more on the object's optical characteristics, such as optical transmittance or optical absorption, rather than its mechanical and physical properties. PAI can "visualize" the light-absorbing chromophores such as hemoglobin, water, and other fluids with desirable penetration depth. Therefore, PAI shows its uniqueness compared to conventional imaging methods. Various information can be visualized through this technique, such as the structure of capillaries, the flow rate of the blood, as well as the temperatures. The accuracy of the PAI resolution can be narrowed from centimeters to micrometers. All these advantages listed above proved photoacoustic imaging (PAI) the wide sorts of applications in medical research, clinical study, cancer/tumors study, and other abnormal diseases [9].

Not only in the field of biomedical but also photoacoustic technology has also been applied in the aspect of engineering innovations. Photoacoustic microscopy, known as PAM, is an application of photoacoustic effect with compounded imaging technology. When a laser or light is incident on the biological material, the energy carried from the laser is transferred to the material and then converted in the form of heat, causing thermal-elastic expansion, and ultrasonic waves to be produced. The relationship between wave intensity and optical absorption is positively proportional to each other [10]. Unlike the conventional technology of optical microscopy, PAM realizes the breakthrough in the field of optical diffusion by using the scattering of the feeble acoustic wave inside the objects. Because of its outstanding precision, images with excellent resolution can be provided by the PAM technology at the imaging scales around millimeters. Significantly, PAM presents practical information and molecular properties simultaneously [11].

### 1.3 Surface Plasmon Resonance (SPR)

The resonant vibration of conduction electrons at the surface between positive and negative permittivity material excited by the incident laser is known as surface plasmon resonance (SPR). SPR plays a crucial role in measuring the light absorption efficiency of metal nanoparticles and planar metal materials such as gold and silver. SPR also plays an important role and acts as the fundamental principle behind many color-based biosensor applications such as biomolecular interactions analysis and photoacoustic imaging.

#### 1.3.1 Surface plasmon resonance in gold nanoparticles

Over the years, the research of gold nanoparticles (AuNPs) has aroused great interest. On the one hand, nano-sized gold materials have been extensively studied in the fields of medical imaging, biosensing, drug delivery, and cancer treatment. On the other hand, the study of AuNPs also shows great value in the aspects of electrical engineering, material science, chemical interaction, and properties of matter's optical nonlinearity [12]. The optical properties of AuNPs have been a hot topic for many years. Advances in the laser field have made the research on the nonlinear optical properties of AuNPs more comprehensive.

To understand the nonlinear optical properties of AuNPs, the introduction of surface plasmon resonance in AuNPs is needed. As shown in Figure 2a, free conductive electrons are polarized due to the electric field generated by the incident laser. Conducting electrons are much lighter than the ionic core in the center of the spherical gold nanoparticle. It is assumed that the positively charged core of AuNPs is stable and fixed, while the negatively charged electrons can move freely, and their movement is affected mainly by the applied electric field. So, the displacement of the negatively charged electrons to the positive side occurs when an applied

electric field is placed around the AuNPs; technically speaking, at the boundaries of the AuNPs, a net charge difference is created. This provides linear resilience to the system. Consequently, the periodic vibration of the electrons is created, known as the surface plasmon resonance in AuNPs [13]. If these AuNPs are dispersed inside the isotropic fluids such as water, their positions and directions of the resonance are entirely random and unpredictable, as shown in Figure 2b.

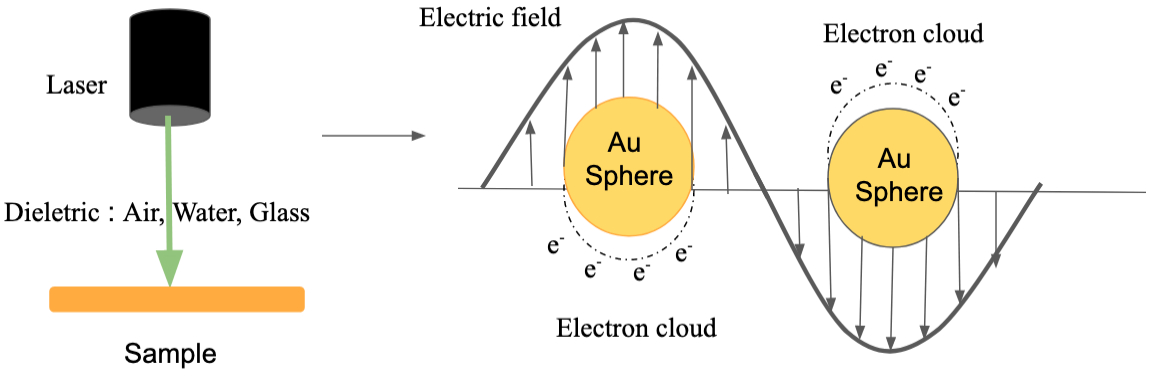


**(a)**

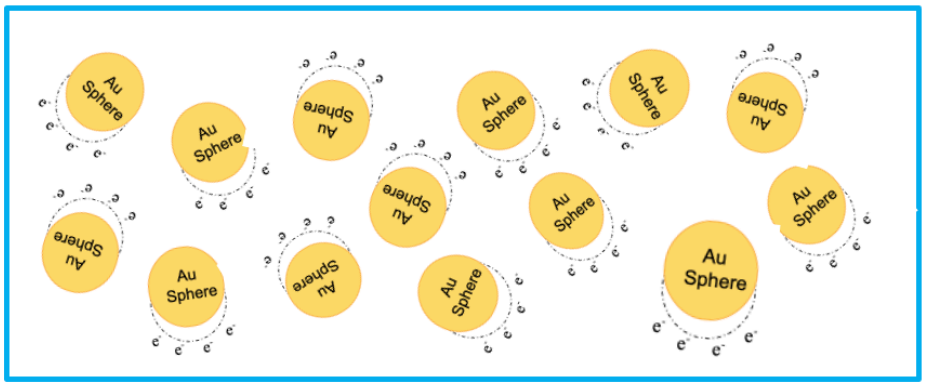


**(b)**

Figure 2: (a) The creation of surface plasmon resonance of Au nanoparticles and (b) surface plasmon resonance of Au nanoparticles in isotropic fluids

### 1.4 Optical Z-scan technique

Some parameters are essential in the field of nonlinear optics. For instance, the third-order nonlinear optical susceptibilities $\chi^{(3)}$is the parameter that plays a significant role in nonlinear optics. As a complex quantity, the real component of $\chi^{(3)}$represents nonlinear refraction ($n_2$) and the imaginary component of $\chi^{(3)}$ represents the nonlinear absorption (β). Hence, the measurement of these parameters is necessary and essential.

The method that widely used to measure the optical nonlinearities of different materials by exciting the sample surface with a direct incident laser is called the Z-scan technique. The closed-aperture Z-scan technique is used to detect the phase change in the nonlinear sample. Moreover, this change helps people to obtain the change in the index of refraction (n). Changes in the nonlinear index of refraction (n) lead to changes in the nonlinear distortions of the laser. A positive Kerr effect leads to self-focusing of the laser beam. In comparison, a negative Kerr effect results in defocusing.

Moreover, the difference in the transmission that is caused by nonlinear absorption is determined by the open-aperture Z-scan technique. It is possible to determine the nonlinear absorption and nonlinear refraction concurrently. Therefore, both real and imaginary parts of third-order nonlinear susceptibility χ (3) can be obtained [14].

Figure 3 shows the schematic of the Z-scan technique. The sample is moved through a focused laser beam in the same direction of propagation of the incident laser, i.e., along the Z-axis. The transmittance of the sample is determined as a function of position Z. The beam splitter reflects a part of the incident laser onto detector 1. The ratio of detector 2 and detector 1 values gives us the normalized transmittance. This method allows determining the nonlinear absorption (β) of the material.

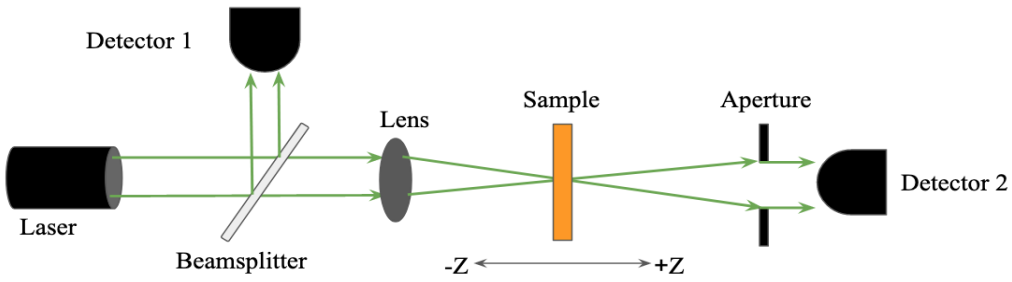


Figure 3: Schematic of conventional Z-scan setup

### 1.5 Nonlinear optical absorption properties

#### 1.5.1 Nonlinear absorption

Nonlinear optical absorption is a phenomenon when an interaction happens between the laser and the material. It also can be described as the absorption coefficient of the medium varies as a function of the light intensity *I*. In some situations, even though there is no linear absorption at a given wavelength, it is possible to observe nonlinear absorption. Occasionally, the absorption can be observed at low intensities, but the absorption can either increase or decrease as the incident intensity increases. The phenomenon with reduced absorption coefficients for increasing light intensity intensities until the coefficient is saturated is called Saturable Absorption (SA) [16]. In comparison, Reverse Saturable Absorption (RSA) is a phenomenon in which the absorption coefficient increases as the intensity of light increases, as shown in Figure 4.

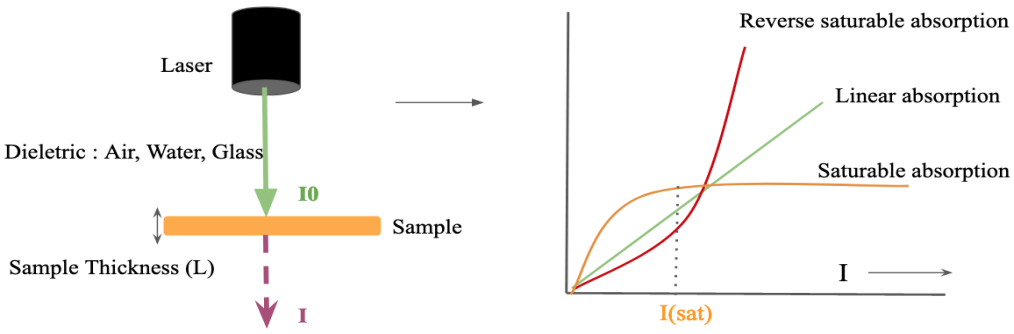


Figure 4: Schematic of linear/nonlinear absorption

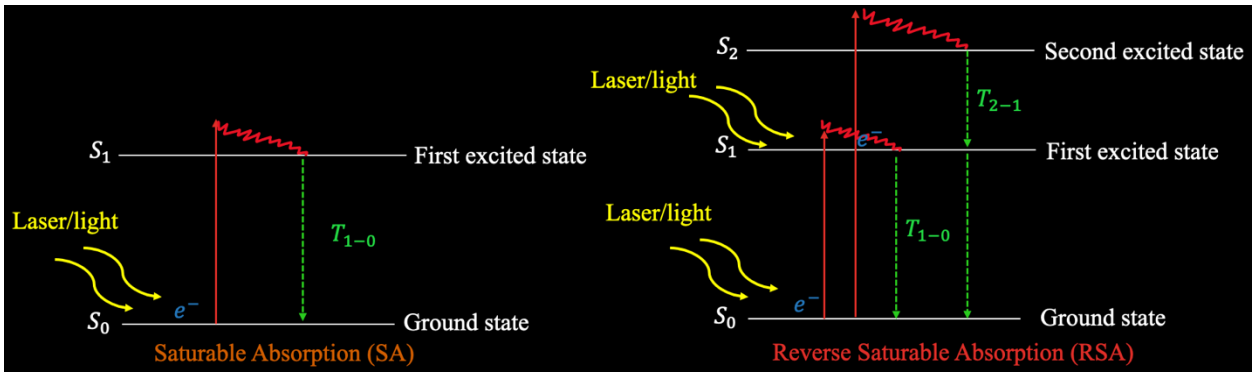


Figure 5: Energy level models of Saturable Absorption (left) & Reverse Saturable Absorption (right)

To understand SA and RSA, energy level model is introduced. A two-energy level model (Figure 5 left) is used to explain saturable absorption. When electrons in the ground state S0 absorb photos or energy from the incident laser, excitation happens, excited electrons will jump to higher energy level S1. Within the lifetime in the first excited state S1, electrons tend to release their energy and back to the lower energy state S0 with relaxation time $T_{1-0}$. As the increasing intensity of the incident laser, the transition process between S0 and S1 becomes periodic and equilibrium, saturate the absorption. In the case of reverse saturable absorption, a three-energy level model (Figure 5 right) is introduced to explain its principle. S2 is a higher energy state known as the second excited state. Similar to saturable absorption, the excitation of electrons due to the energy absorption from incident laser leads the energy level changes from S0 to S1 and then S1 to S2. Because the relaxation time $T_{2-1}$ is longer than $T_{1-0}$ , excited-state absorption (S1 to S2) happens. Thus, the growing intensity of the incident laser increases the absorption of the system. Two-photon absorption (TPA) is another type of RSA. In two-photon absorption, energies of two photons will combine to excite a single electron from a lower energy state (ground state S0) into a higher energy state (excited state S1). In some cases, for instance, at high intensity, the absorption can still happen even though the energy of one photon is not enough to

cross the bandgap [16]. The energy that the two photons absorb to get the excited state equals the energy difference between the ground state and the excited state. Similarly, multiphoton absorption happs when more than two photons are involved in this process. The laser energy storage may realize under the peak powers and intensity reached in the short pulses [17].

### 1.5.2 Open aperture Z-scan nonlinearities

As discussed previously, the nonlinear absorption coefficient can be determined directly by using open aperture Z-scan technique. For the transmittance *T(Z)*:

$$T(Z) = \sum_{i=0}^{i=\infty} \frac{\left(-\beta I(Z) L_{eff}\right)^{i}}{(i+1)^{\frac{3}{2}}} \tag{1.5.1}$$

where β is nonlinear absorption. $I(Z)$ is the irradiance (power per unit area):

$$I(Z) = \frac{I_0}{(1+\frac{z^2}{z_R^2})} \tag{1.5.2}$$

$$I_0 = \frac{E_p}{\tau\lambda} \tag{1.5.3}$$

where $Z_R$ in equation (1.5.2) is the Rayleigh range of the beam, $I_0$ is peak on-axis irradiance at the focus, $E_p$ is pulse energy of the laser, λ is the wavelength of the laser and τ is the pulse width, and $L_{eff}\ the$ is the effective length of the sample:

$$L_{eff} = \frac{1-e^{-\alpha L}}{\alpha} \tag{1.5.4}$$

where the α is linear absorption coefficient and L is the sample thickness. To simplify the transmittance *T(Z)*, we only consider the first and second-order of the equation of transmittance, when $i = 0$ and $i = 1$.

$$T(Z) = 1 - \frac{\beta I(Z) L_{eff}}{2^{3/2}} \tag{1.5.5}$$

### 1.5.3 Photoacoustic Z-scan (PAZ-scan)

The Z-scan technique is widely used in nonlinear optics in understanding the characteristics of nonlinearity of a wide variety of materials. Synchronously, the growing fabrication of increasing novel nanostructure products enabled us to understand the relation between the particle sizes and their nonlinear optical properties.

Photoacoustic Z-scan (PAZ-scan) technique integrates the advantages of the conventional Z-scan technique and the high sensitivity of photoacoustic detection. In addition to recording the transmitted optical (OPT) signal as done in conventional Z-scan, we also measure the photoacoustic (PA) signal using an ultrasound transducer as the sample is moved along the Z-direction. The intensity of the PA signal is linearly dependent on the optical absorption, the magnitude of the photoacoustic signal P(Z):

$$P(Z) = \Gamma \alpha I(Z) \tag{1.5.6}$$

where $I(Z)$ is the intensity of the incident laser, Γ is the Gruneisen coefficient and α is the absorption coefficient. When the samples depict nonlinear absorption, then $\alpha = \alpha_0 + \beta I$, and the equation (1.5.6) becomes, the normalized photoacoustic signal $P_{normal}(Z)$ as:

$$P_{norm}(Z) = 1 + \frac{\beta}{\alpha_0} \frac{E_p}{\tau \lambda Z_R (1 + (\frac{Z}{Z_R})^2)} \tag{1.5.7}$$

where $E_p$ is pulse energy of the laser, λ is the wavelength of the laser, τ is pulse width and β is nonlinear absorption.

### 1.6 Liquid crystal

First discovered in 1888 by Friedrich Reinitzer, an Austrian botanical physiologist, liquid crystals are known as the condensed matter with the properties in between traditional liquids and solids. For example, the direction of the liquid crystal molecules can be oriented like the molecules are oriented in a crystal. However, at the same time, the liquid crystals present similar properties to liquid. One of the most interesting characteristics of liquid crystals is their changeable phase, dependent on the temperature. As the temperature increases, the liquid crystal phase will change from a liquid crystal state (anisotropic) to a transparent liquid state (isotropic phase) like water. Most importantly, these phase differences can be studied via their optical properties.

#### 1.6.1 Nematic liquid crystal

The nematic phase has been known as one of the most common phases of liquid crystals. Molecules inside the nematic phase liquid crystal are oriented in a preferred direction (ñ), as shown in figure 6. The word “nematic” also means "thread" in Greek. This term initially comes from the observation of the thread-like topological defects in the nematic phase. The nematic liquid crystal also shows the characteristic of so-called “hedgehog” topological defects [18]. In the nematic phase, the rod-shaped liquid crystal molecules have no positional order, but self-align and parallel to the direction (ñ) [18].

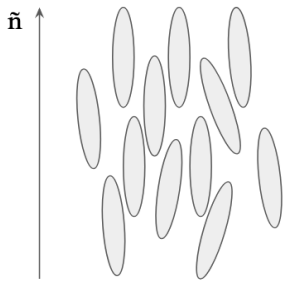


Figure 6: The schematic of Nematic liquid crystal molecule’s orientation

In both the industry and medical fields, the application of nematic liquid crystals is widely used. To study different materials' structural properties and inhomogeneities in the field of science, nematic liquid crystals are wieldy used for the detection. This nondestructive, highly sensitive technique allows the visualization of invisible peculiarities of the surface examined. Recently, the applications that use the properties of nematic liquid crystals to decorate and image biological or medically important samples are playing an increasingly important role in the medical and biological field [19].

### 1.6.2 SPR of gold nanoparticles in nematic liquid crystal

As mentioned in section 1.3.1, as an isotropic fluid, the alinements of water molecules are sprawling. Therefore, if AuNPs are dispersed in water, then their position and the direction of surface plasmon resonance (SPR) are entirely random and unpredictable. However, when AuNPs are dispersed in nematic liquid crystals, their directions position and the direction of SPR are dictated by the arrangement of the liquid crystal molecules, as shown in Figure 7. This effect can be observed when the liquid crystals are oriented or randomly ordered. Two patterns of LC samples are performed in this study: Planar-oriented and Planar-degenerated. Gold nanoparticles dispersed in the planar-oriented sample are aligned in a preferred direction (Figure 7b), whereas AuNps in degenerated samples are distributed randomly. For both cases, The SPR direction of gold nanoparticles is well organized in 1D. The influence of different sample patterns on sample nonlinearity is discussed in the last section.

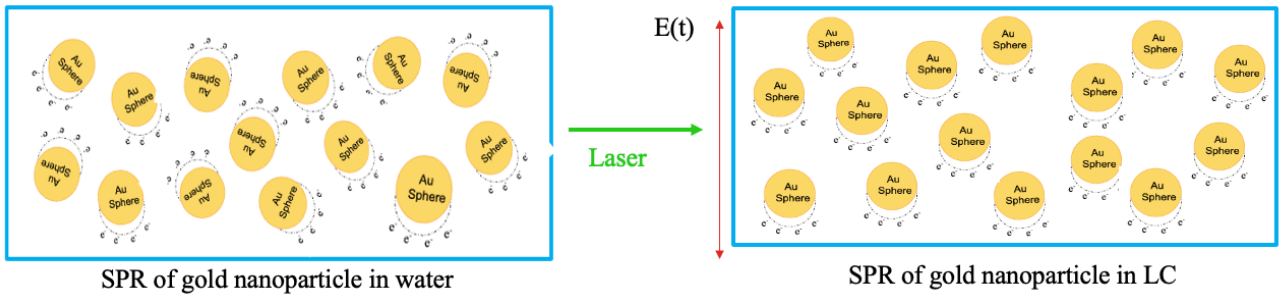


**(a)**

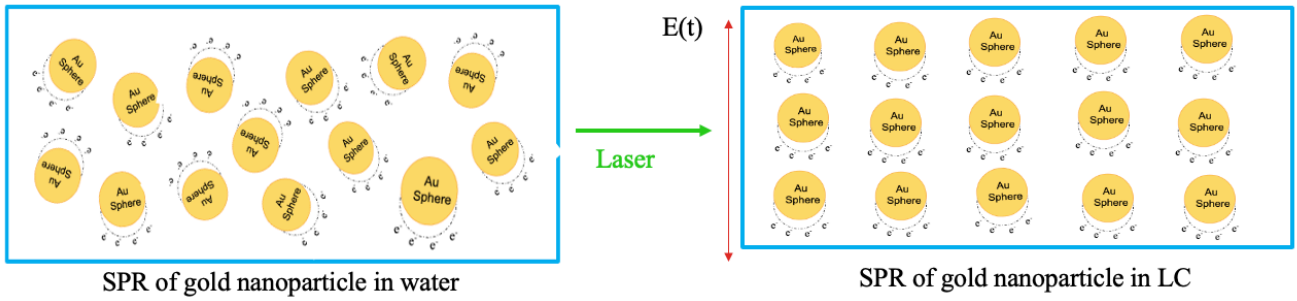


**(b)**

Figure 7: (a) SPR of gold nanoparticles in Planar-Degenerated sample and (b) SPR of gold nanoparticles in Planar-Oriented sample

CHAPTER 2

# 2. EXPERIMENT SETUP

## 2.1 Materials

To study the nonlinear optical characteristic of gold nanoparticles (Au NPs) dispersed within the nematic liquid crystal, 4 types of gold particles are utilized in this work. These chemicals are shown in Table 1 and Figure 8.

Table 1 Information of samples

| Name | Material information |
|---|---|
| G20 | SIGMA-G1652, 20nm Colloidal Gold |
| G10 | SIGMA-G1527, 10nm Colloidal Gold, $0.75A_{520}$ |
| G5 | SIGMA-G1402, 5nm Colloidal Gold |
| G20L | NN-LabsGoldNanocrystals, 20 nm Gold with citrate ligands |
| LC5CB | Frontier Scientific-4-Cyano-4'-n-pentylbiphenyl, 99% 5G |


Figure 8: Material used (G20, G10, G5, G20L, LC5CB)

All unconjugated gold colloids samples (G20, G10, G5) contain approximately 0.01% $HAuCl_4$ suspended in 0.01% tannic acid with 0.04% trisodium citrate, 0.26 mM potassium carbonate, and 0.02% sodium azide as a preservative. G20L contains a similar formula but it includes citrate ligands to prevent the aggregation of the gold nanoparticles in the sample.

**2.2 Sample preparation**

To disperse AuNPs in liquid crystals, water in which AuNPs were suspended was evaporated and mixed with ethanol. Then 5CB nematic liquid crystal solution was mixed with the ethanol-gold NPs solution. The mixture was then heated to evaporate the ethanol to obtain gold nanoparticles in nematic liquid crystals.

To study and compare the nonlinear optical characteristics of gold nanoparticles (AuNPs) (with/without ligands) dispersed in nematic liquid crystals, we prepared two types of liquid crystal cells – planar oriented and planar degenerate (non-oriented). At first, glass plates (Fisher brand microscope slides, 25x75x1.0mm) were cleaned with acid, washed with water, and dried with air to remove water on the surface. Then they are spin-coated on one side with one weight percent PVA solution: (one weight percent PVA = 90% of water + 10% of ethanol + 1% of PVA). Then the glass plates are heated in the oven at 110℃ for at least an hour. To make planar-oriented liquid crystal cells, PVA coated side was rubbed with cloth in one direction. Then a 100 μm spacer was placed between the two glass plates, and the sample (gold NPs doped with nematic liquid crystal) is injected into the cells. The whole thing was sealed with optical glue and cured under UV light. For planar degenerated (non-oriented) cells, we skip the rubbing part.

Pure gold nanoparticles solution cells:

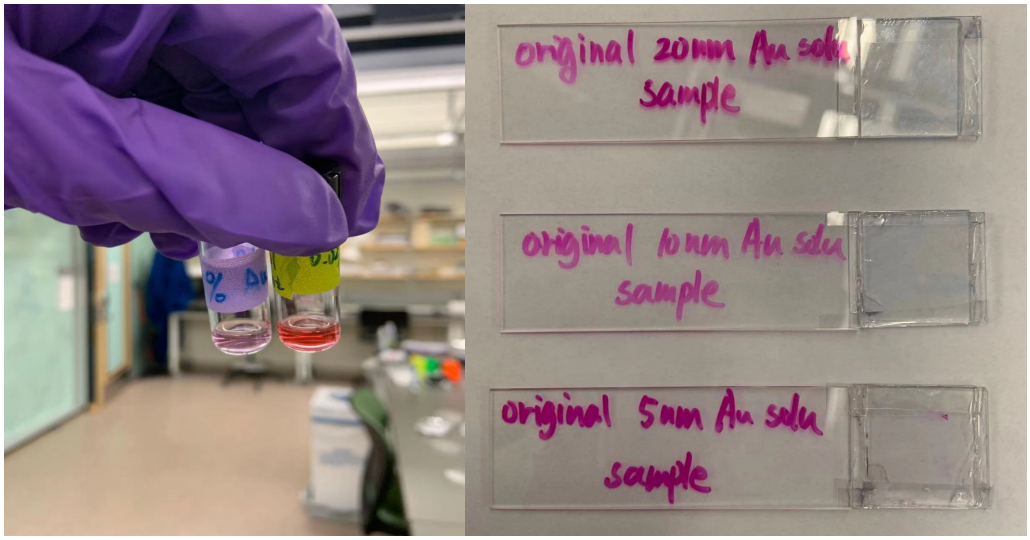


Figure 9: Samples of pure gold nanoparticles solution cells

Materials G20, G10, and G5 are sealed directly inside the glass cells with the spacer thickness equal to 200 μm, respectively.

Gold nanoparticles (with/without ligands) dispersed in nematic liquid crystals:

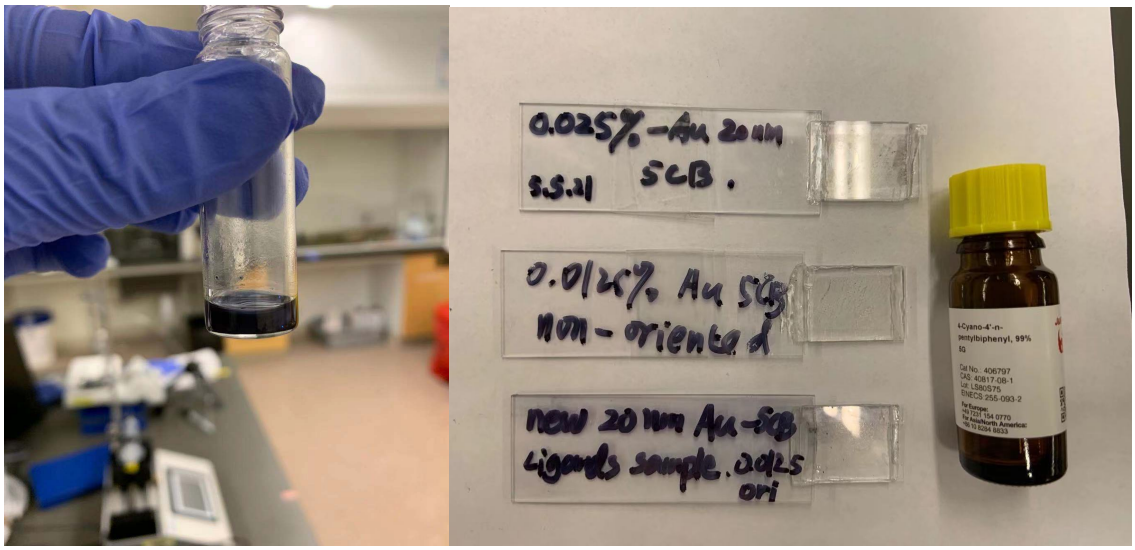


Figure 10: Samples of gold nanoparticles dispersed in nematic liquid crystals

## 2.3 Polarizing microscope

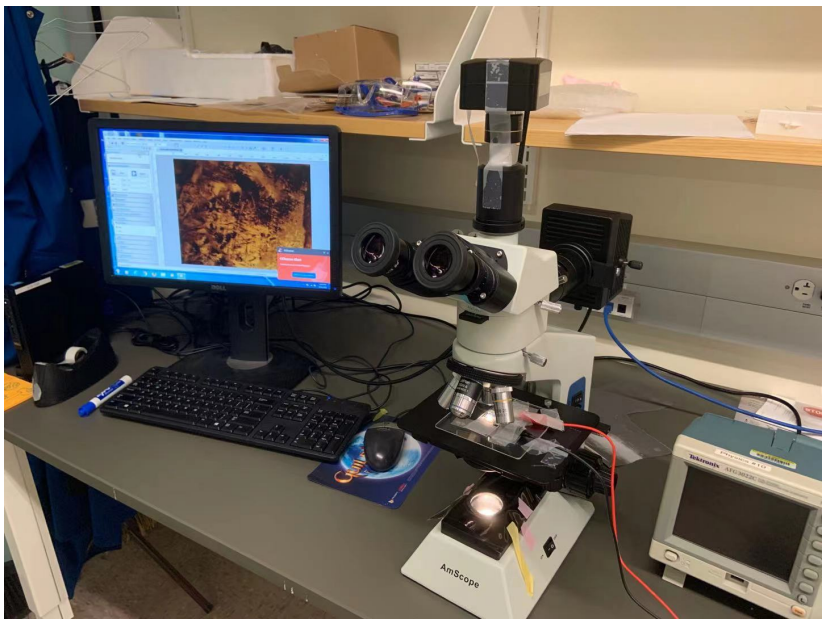


Figure 11: The schematic of the Polarizing microscope

The polarizing microscope is widely used for determining the object's optical characteristics. It is commonly used for anisotropic materials (like liquid crystals) because of their birefringent optical properties – multiple refractive indices. Using polarizing microscopes, scientists can study and understand the molecular order and characteristics in various materials such as condensed matter and living cells [20]. In this experiment, the polarizing microscope was used to study the optical characteristics of the sample cells under different concentrations and the difference between liquid crystals vs. water as a medium.

## 2.4 UV-Vis Optical absorption Spectrum

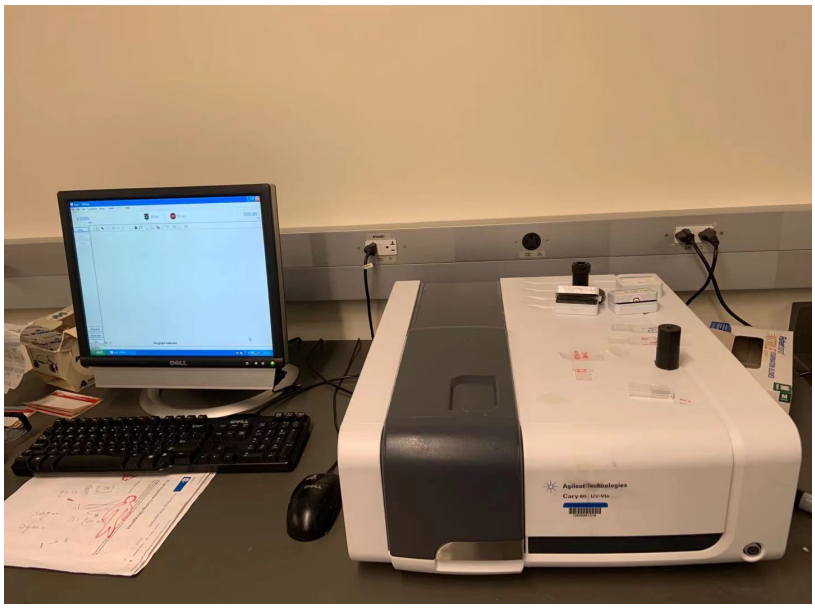

Figure 12: Cary 60 UV-Vis

To determine the linear absorption coefficient, absorbance is needed. In this study, the absorbance was measured using UV-Vis optical spectrum obtained with Cary 60 UV-Vis (Agilent technology from 200-800 nm), shown in Figure 10. Using Beer-Lambert law and the absorbance as a function of wavelength (nm), the absorption coefficient was obtained for all the samples [21].

## 2.5 Photoacoustic Z-scan setup

All samples were studied using optical photoacoustic Z-scan technology. Frequency-doubled (532 nm wavelength, 3 ns pulse width) Nd:YAG laser (Minilite II) is used as the light source. The laser is focused on the sample using a 20 cm focal length lens. The sample was placed at 45 degrees with respect to the incident laser inside a custom-made module that contains water for PA signal transmission. The entire system is carefully aligned on the (Thorlabs NRT 150) XYZ translation stage to collect the PA/OPT signal. As the sample is excited by

the incident laser pulse, energy from the laser is absorbed and converted into heat. This leads to the result of the photoacoustic effect and thus generates ultrasonic emissions. Then, ultrasonic waves are detected by  (Olympus NDT U8423240) 10 MHz focused water immersion transducer. An optical detector is used to measure the energy transmitted through the sample. The light source waveform is stabilized by a trigger (Model 818-BB-21A). The module is translated along the propagation direction of the laser beam. All PA/OPT signals and data are collected using the LabView program (see Figure 14). The resulting experimental measurements were then plotted and fitted on the nonlinear equation and the best fitting nonlinear absorption coefficient values are obtained.

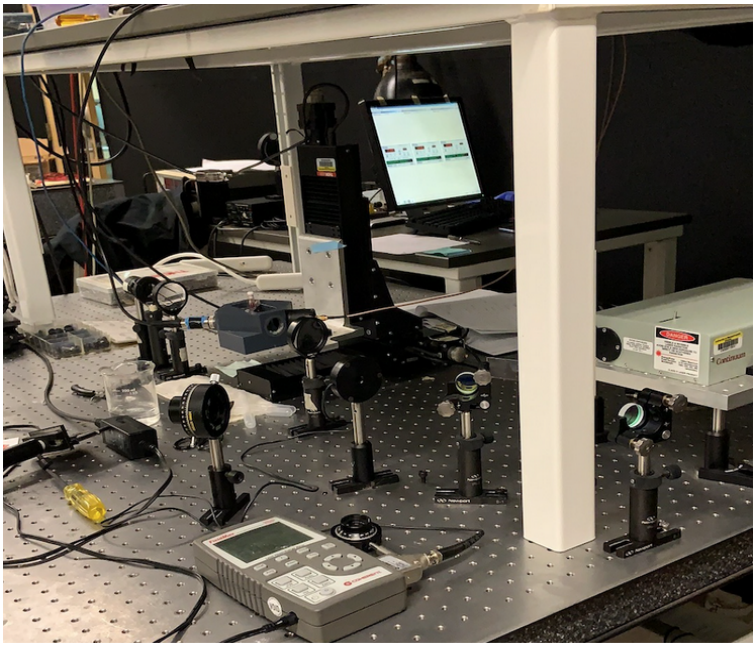

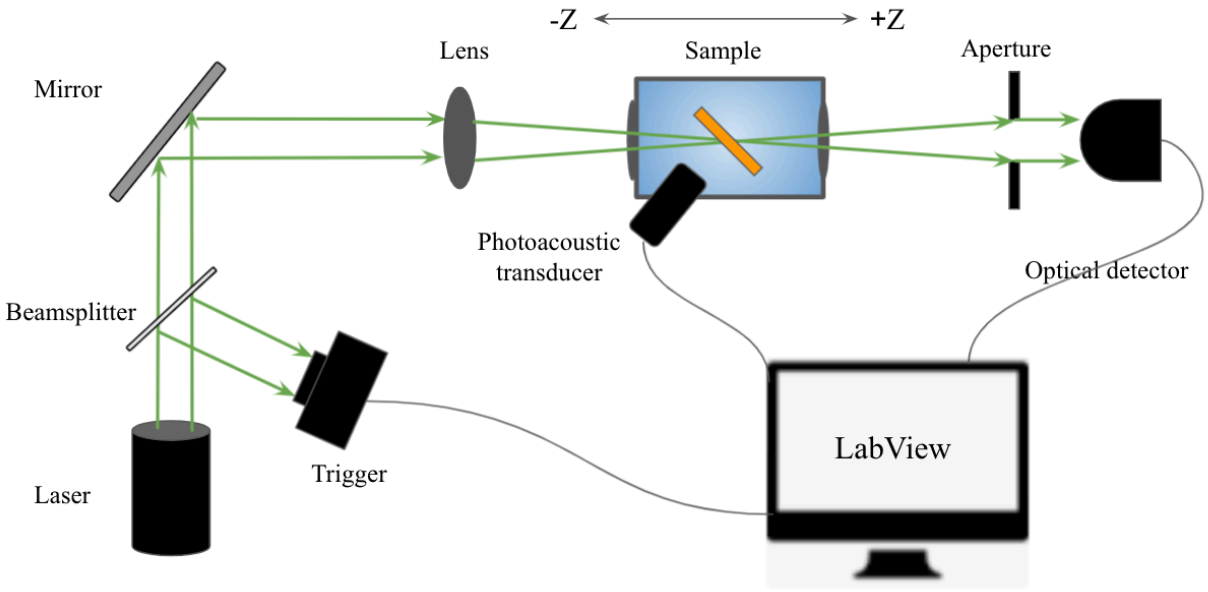


Figure 13: Real PAZ-scan setup

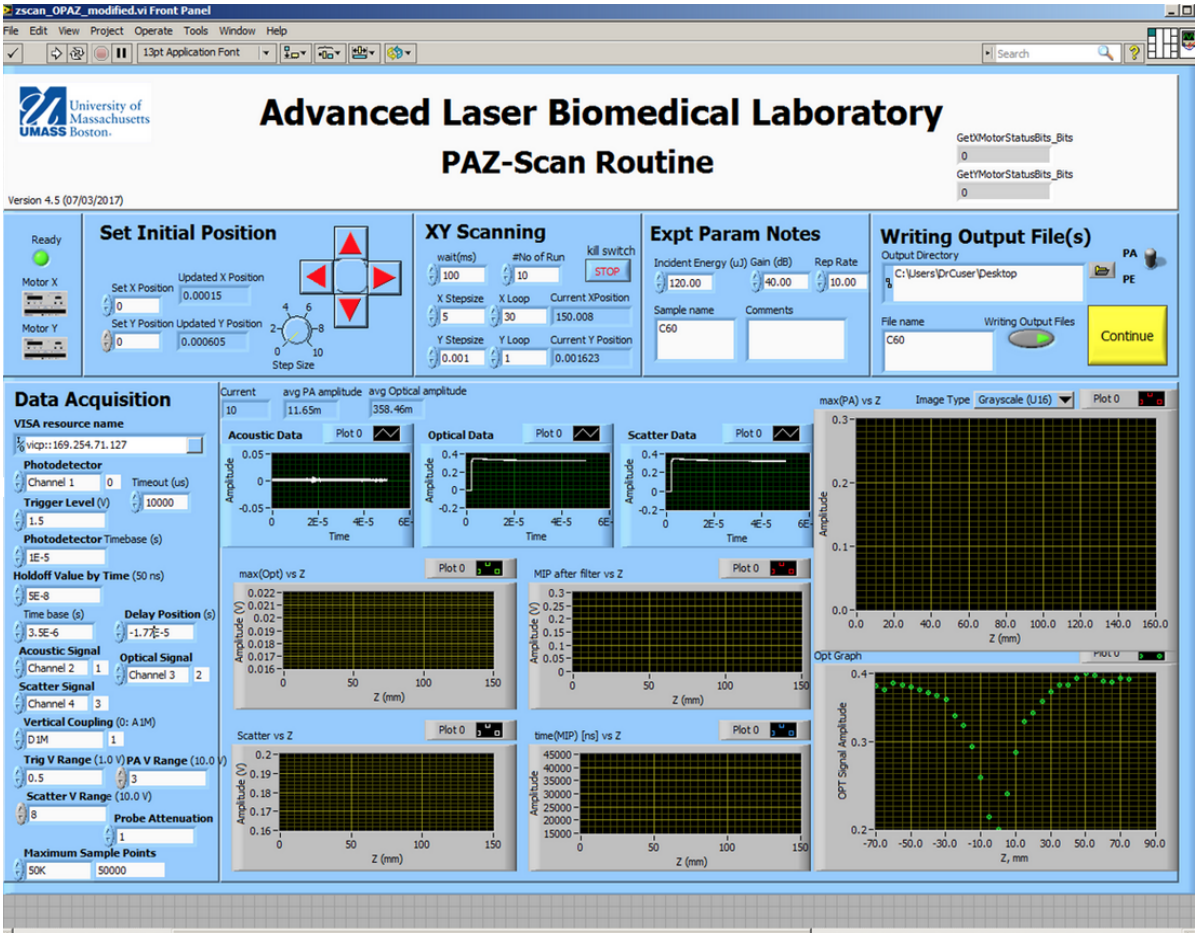


Figure 14: Interface of LabView

CHAPTER 3

# 3. RESULT & DISCUSSION

## 3.1 Imaging using the polarizing microscope

### 3.1.1 Liquid crystals vs Water as medium

A polarizing microscope (AmScope) is used to understand the fundamental optical properties of the samples. In order to visualize the difference between the samples and figure out how the liquid crystals, which act as the medium in which gold nanoparticles are dispersed, will influence the sample's optical characteristic, we analyze the samples cells (Pure gold nanoparticles solution cells and Gold nanoparticles doped with liquid crystals) under the bright field and the crossed polarizers.

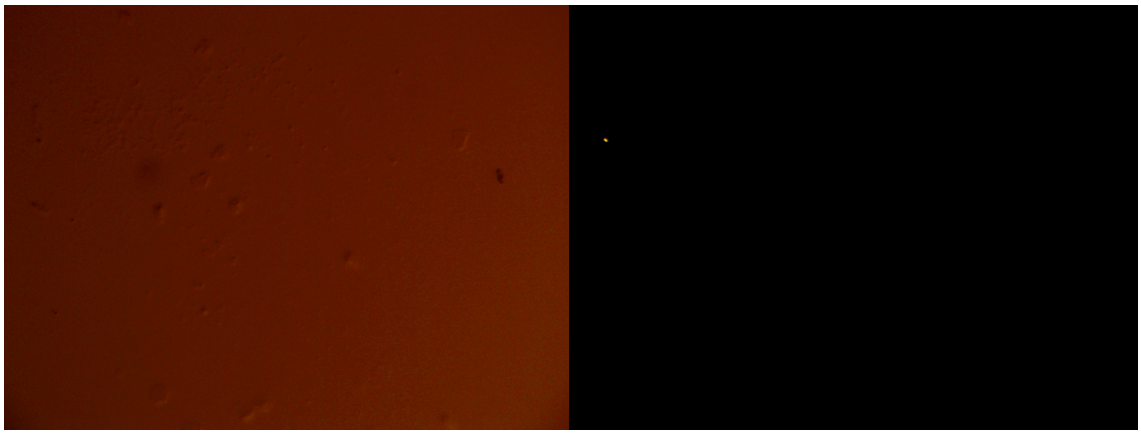

**(a)** **(b)**

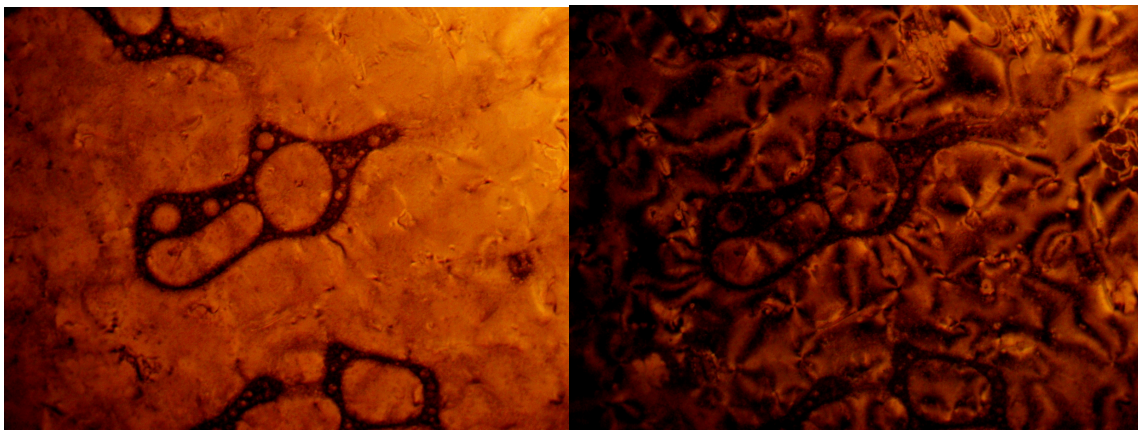

**(c)** **(d)**

Figure 15: Sample of pure gold nanoparticles (solution without ligands) under (a) bright field, and (b) crossed polarizer; Sample of gold nanoparticles (without ligands) doped with liquid crystals under (c) bright field, and (d) cross polarizer.

Figure 15 shows the main difference between water and liquid crystals that act as the medium for the gold nanoparticles. When water was used, the gold particles dispersed evenly, as can be seen under the bright field microscope (Figure 15a). Hence nothing is observed under the crossed polarizers. This is because water is an isotropic fluid; light is blocked/filtered by the crossed polarizer (Figure 15b). On the other hand, when liquid crystals are used, big aggregations of the gold particles were formed since the gold nanoparticles without legends tend to aggregate together (Figure 15c). Also, the anisotropic properties of liquid crystals at room temperature enable light to pass through the cross polarizer to visualize the phase defects (Figure 15d).

### 3.1.2 Planar-oriented Vs. Planar-degenerated

In this section, the differences between planar-oriented cells and planar-degenerated cells (under crossed polarizers) are discussed. For the planar-oriented liquid crystal cells, glass plates with PVA coating are rubbed with cloth in one direction (while for planar-degenerated cells, no rubbing is performed). The liquid crystals, hence the nanoparticles, tend to be

oriented along the rubbed lines. Therefore, we observed uniform and evenly dispersed nanoparticles in planar-oriented cells under the brightfield illumination (Figure 16a) compared to those in planar-degenerated cells (Figure 16b). To observe the characteristic of oriented cells and degenerated cells in the isotropic phase, samples are heated up to $50^0$C to realize the phase change from anisotropic to near isotropic. When samples are in the isotropic phase, the "crystal" like structure vanishes and the dispersion of the gold nanoparticles can be seen more clearly. The dark dots and spots in images Figure 16c and 16d are the gold nanoparticles dispersed in the liquid crystals. In the isotropic phase, the gold particles dissolve nicely and uniformly in the oriented cells (Figure 16c). For gold particles in degenerated cells, they disperse less uniformly and form some aggregations (Figure16d). When the temperature is decreased to room temperature, the "crystal-like" structure reappears (Figure 16e and 16f). The gold nanoparticles aggregate in planar-degenerated cells since no rubbing was involved. Therefore, the gold nanoparticles are dispersed in the liquid crystal without any organized pattern and hence tend to stay together (Figure 16f). In comparison, at room temperature, the gold nanoparticles show a good arrangement in the planar-oriented cells (Figure 16e). The influence of the dispersion of the gold nanoparticles within the samples cannot be neglected since this will also affect the PA and OPT signal detected by using the Z-scan technique; details will be discussed in the following sections.

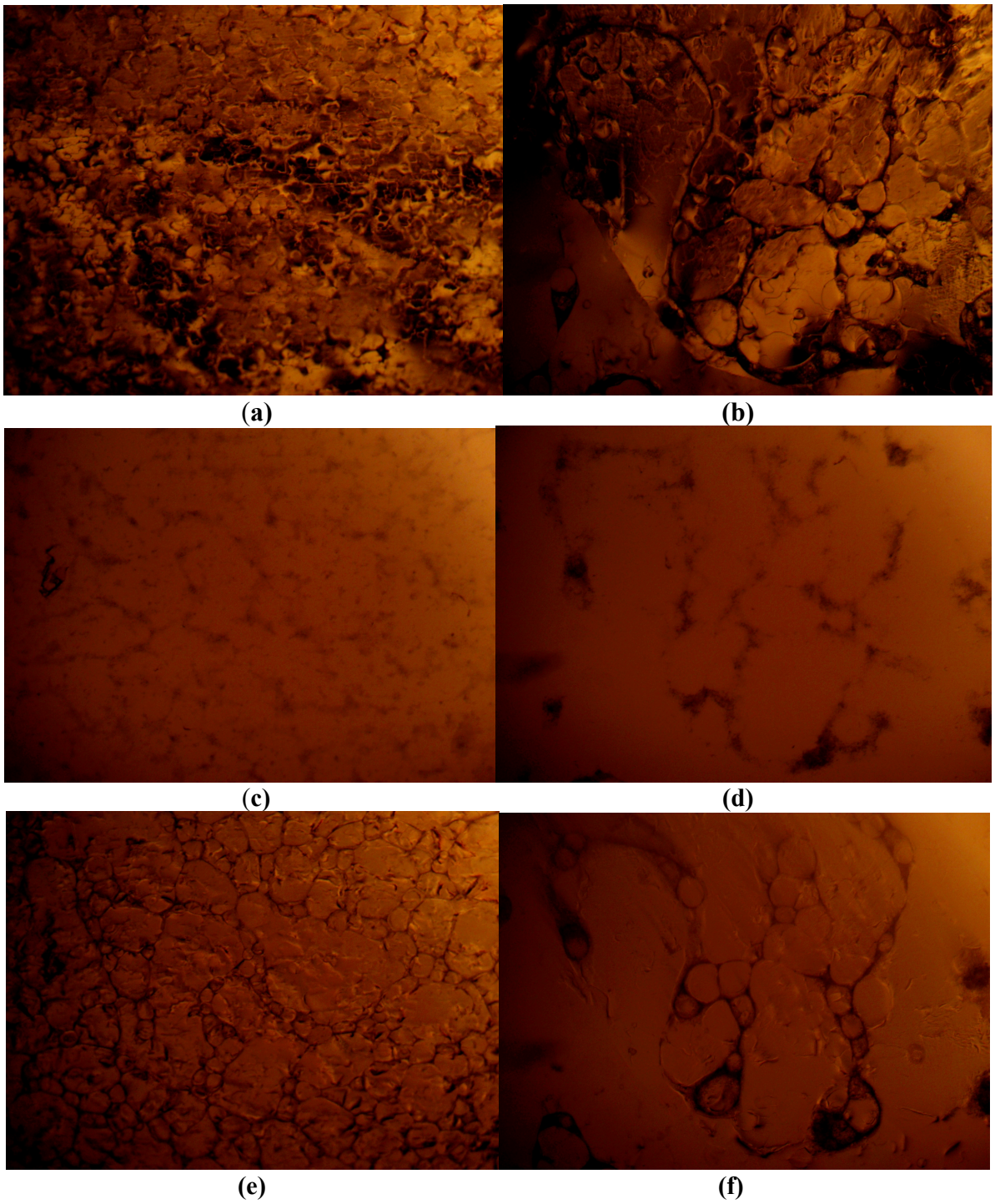


Figure 16: Images under cross polarizer: (a) planar-oriented liquid crystal cell, (b) planar-degenerated liquid crystal cell; Images of samples after been heated, near isotropic phase: (c) planar-oriented liquid crystal cell and (d) planar-degenerated liquid crystal cell; when sample's temperature cools down to room temperature, the images of (e) planar-oriented liquid crystal cell and (f) planar-degenerated liquid crystal cell.

### 3.2 Absorbance and absorption coefficient

UV-Vis absorption spectra of the samples were measured by Cary 60, as depicted in Figure 17. Figure 17a shows the absorption spectra of gold nanoparticles of 5 nm and 20 nm. The absorbance difference between planar-oriented LC5CB sample and planar-degenerated LC5CB sample is shown in Figure 17b. The oriented samples have better absorbance than degenerated samples under the same gold concentration for all wavelengths. Because for planar degenerated (non-oriented) cells, we skip the rubbing part, leading to the unrestricted positioning of the molecules of liquid crystals. This causes the gold nanoparticles to disperse randomly and formed aggregations inside the cells, as shown in Figure 16f. In comparison, as shown in Figure 16e, gold nanoparticles dispersed evenly and uniformly in planar-oriented cells. The higher the concentration, the greater the absorbance for the oriented LC5CB samples under the different gold concentrations in Figure 17c.. Under the same gold concentration, samples made with liquid crystals-based solvent have much higher absorbance than samples made with water-based solvent (Image 17e, Image 17f, Image 17g). Moreover, from Figure 17h, it is evident that for all liquid crystals-based samples, absorbance is more compared with water-based samples under various gold concentrations.

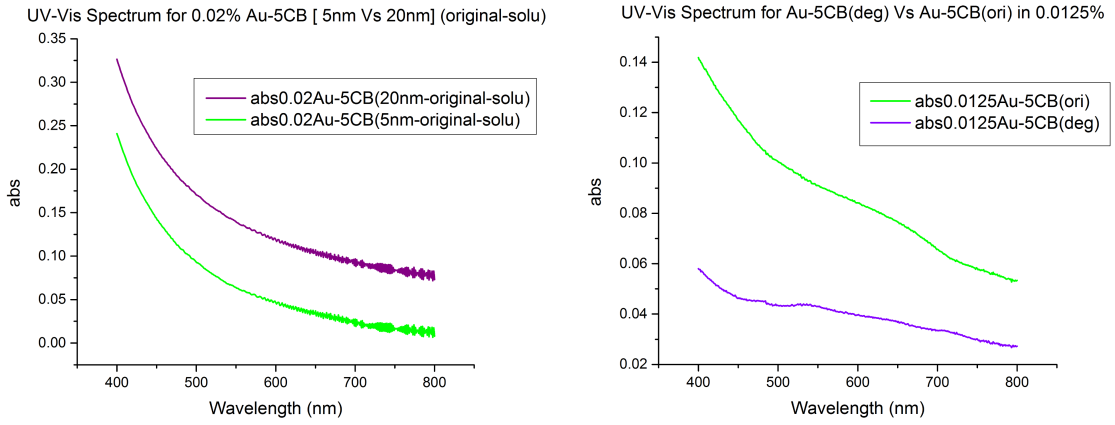


**(a)** **(b)**

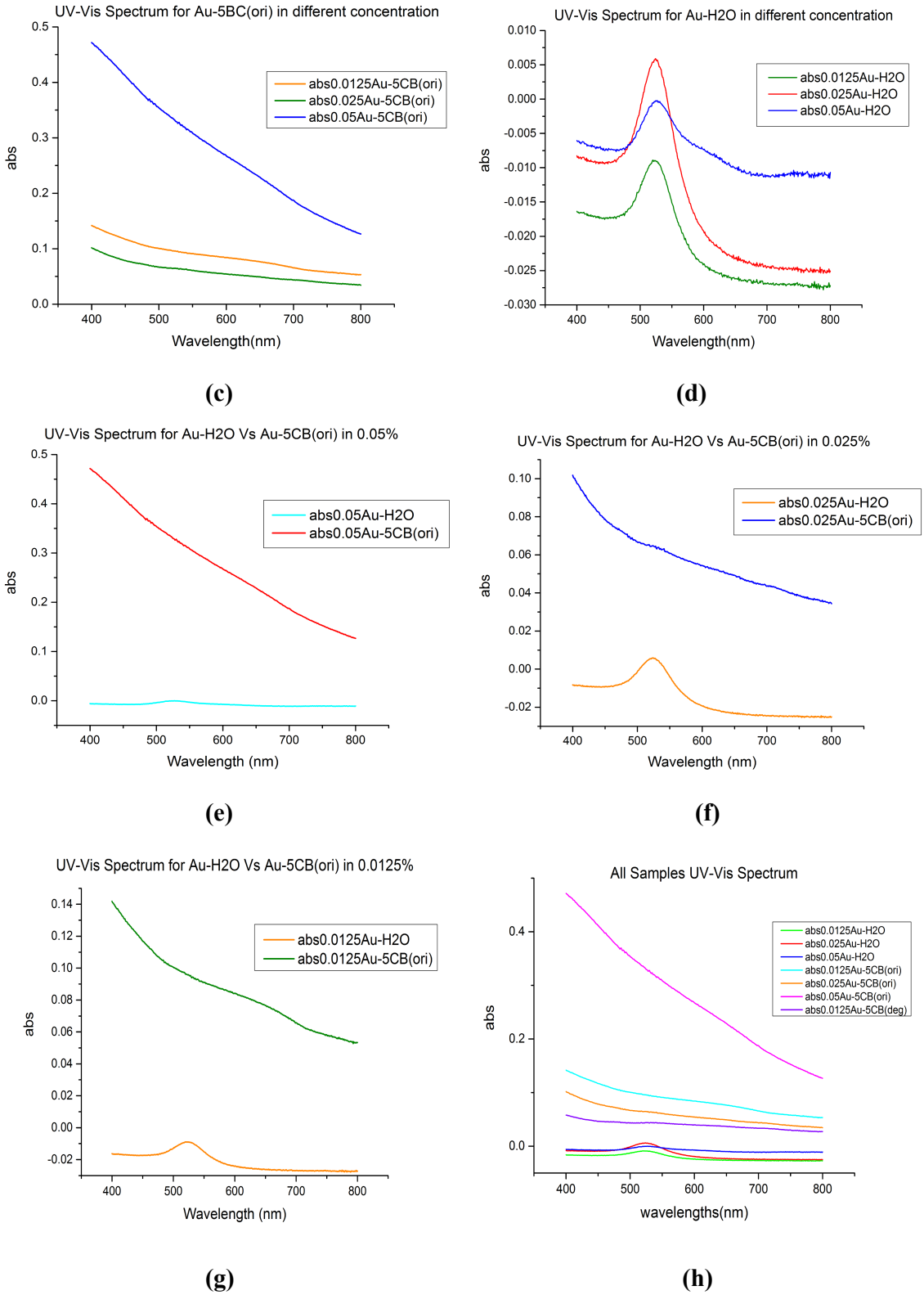


Figure 17: UV-Vis spectrum for all samples

Using the UV-Vis spectrum, the absorption coefficient ($\alpha_0$) was calculated. Appling Beer-Lambert law $\alpha_0$=2.303(abs)/t, the linear absorption coefficient can be calculated (abs represent the absorbance at the wavelength at 532 nm for each sample and *t* represents the sample's thickness = 100 μm). Samples' absorbance and linear absorption coefficient are presented in Table 2.

Table 2 Absorbance and linear absorption of all samples

| **Sample** | **abs** | **$\alpha_0$ ($m^{-1}$)** |
|---|---|---|
| 0.0125%-20nmAu-H2O | 0.00973 | 223.985 |
| 0.025%-20nmAu-H2O | 0.00448 | 103.1296 |
| 0.05%-20nmAu-H2O | 0.00054 | 12.4308 |
| 0.0125%-20nmAu-5CB (ori) | 0.09433 | 2171.477 |
| 0.025%-20nmAu-5CB (ori) | 0.0639 | 1470.978 |
| 0.05%-20nmAu-5CB (ori) | 0.32379 | 7453.646 |
| 0.0125%-20nmAu-5CB (deg) | 0.044 | 1012.88 |
| 0.02%Au-5CB(ori) [20nm-original-solu] | 0.14968 | 3445.634 |
| 0.02%Au-5CB(ori) [5nm-original-solu] | 0.07268 | 1673.094 |

### 3.3 Photoacoustic and optical signal

The nonlinear characterizations of the liquid crystals-based samples were carried out for three gold concentrations: 0.05 weight percent, 0.025 weight percent & 0.0125 weight percent. We also varied the pulse repetition rate of the laser to 2 Hz, 5 Hz, and 10 Hz to understand how the concentration of the gold nanoparticle and laser frequency will affect the nonlinearity. All liquid crystal-based samples (planar-oriented & planar-degenerated) are studied using the open-aperture optical and photoacoustic Z-scan technique.

### 3.3.1 Photoacoustic/optical signal and nonlinear coefficient β under 10Hz

To obtain the graph of photoacoustic/optical signals as well as the nonlinear coefficient (β), data from LabView is collected and plotted as shown in figures 18(a) and 18(b). The Y-axis is the normalized value for PA/OPT signal and, X-axis is the position of the sample along the Z-direction. Along the z-axis, the intensity I(Z) is optimum at the focus (Z=0) and decreases gradually on either side, following the Gaussian profile, as resembles by equation 1.5.2. All the samples show reverse saturable absorption property – absorption increases as intensity is increased. Since the PA signal is linearly proportional to the absorption, the PA signal increases with intensity (see section 1.5.1). Thus, we see a complementary signal between PAZ-scan and optical Z-scan, as depicted in figures 18(a) and 18(b). Figures 18(c) to 18(j) show the PAZ and optical Z-scans for each concentration and liquid crystal orientation and the best fit to the experimental results using equations 1.5.5 and 1.5.7. The plots for normalized PA/OPT signals fit well to the experimental data, with the curve showing the minimum error points. The value of the nonlinear coefficient (β) can be obtained from the curve fitting and shown in Table 3 below. Clearly, the value of β is more at low concentrations.

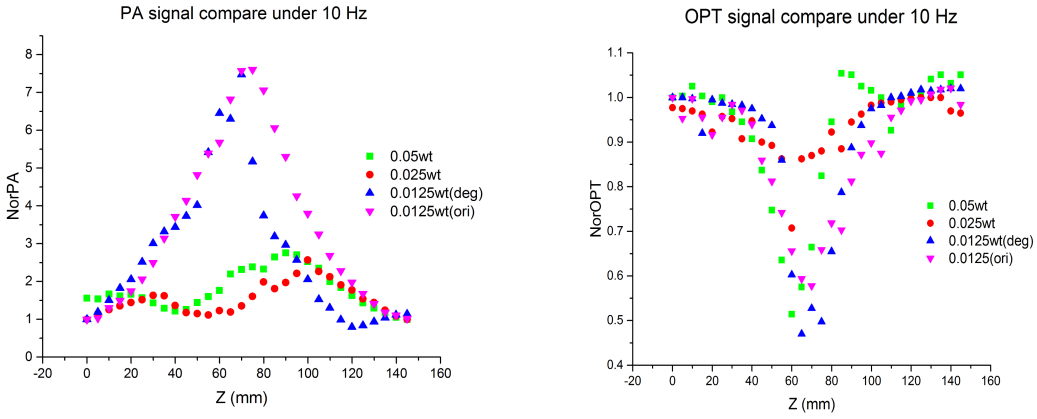


**(a)** **(b)**

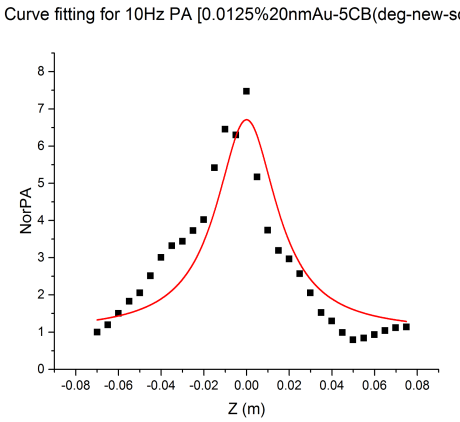
Curve fitting for 10Hz PA [0.0125%20nmAu-5CB(deg-new-solu)]
NorPA
Z (m)

**(c)**

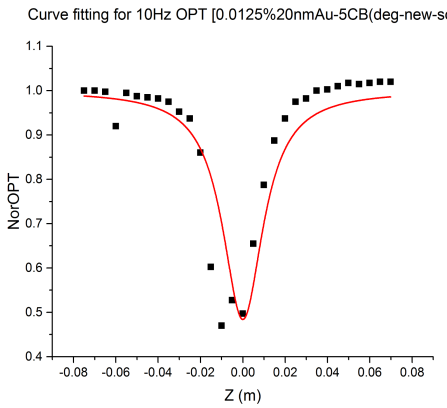
Curve fitting for 10Hz OPT [0.0125%20nmAu-5CB(deg-new-solu)]
NorOPT
Z (m)

**(d)**

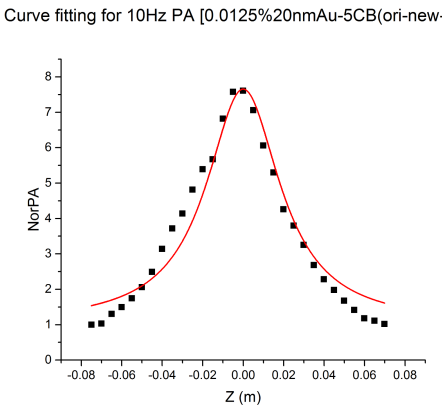
Curve fitting for 10Hz PA [0.0125%20nmAu-5CB(ori-new-solu)]
NorPA
Z (m)

**(e)**

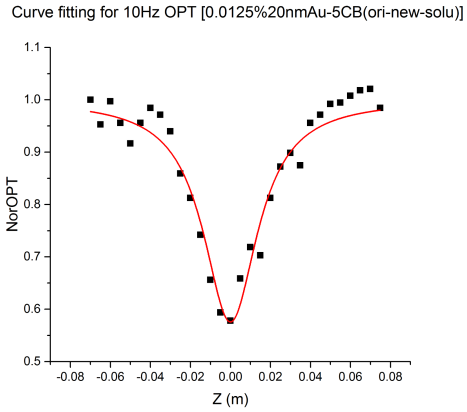
Curve fitting for 10Hz OPT [0.0125%20nmAu-5CB(ori-new-solu)]
NorOPT
Z (m)

**(f)**

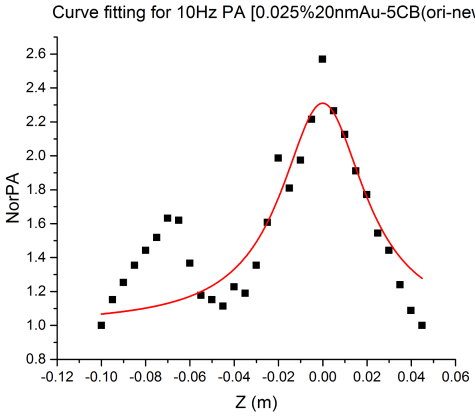
Curve fitting for 10Hz PA [0.025%20nmAu-5CB(ori-new-solu)]
NorPA
Z (m)

**(g)**

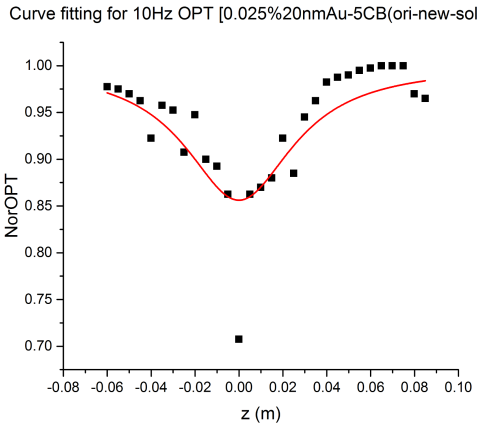
Curve fitting for 10Hz OPT [0.025%20nmAu-5CB(ori-new-solu)]
NorOPT
z (m)

**(h)**

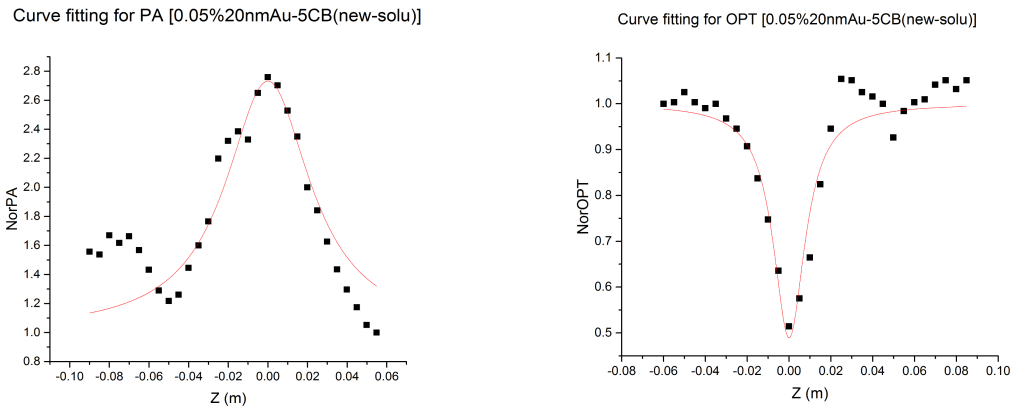


**(i)** **(j)**

Figure 18: Curve fitting and PA/OPT signal under 10 Hz

Table 3 Values of nonlinear coefficient of different samples under 10Hz

| Samples | $\alpha(m^{-1})$ | $\beta$ (W/m) |
|---|---|---|
| 0.05%-20nmAu-5CB(ori) | 7453.646 | $9.23\times10^{-9}$ |
| 0.025%-20nmAu-5CB(ori) | 1470.978 | $1.23\times10^{-9}$ |
| 0.0125%-20nmAu-5CB(ori) | 2171.477 | $8.80\times10^{-9}$ |

### 3.3.2 Photoacoustic/optical signal and nonlinear coefficient β under 5 Hz

In this section, all samples' behavior at 5 Hz laser pulse frequency is discussed. Figure 19 depicts the Z-scan curves and the curve fitting to the experimental data. For sample [0.05%-20nmAu-5CB(ori)], we are unable to get good result. So, it is not discussed. Figure 19a and Figure 19b show that the low gold concentration leads to better PA/OPT plots and fitting curves. Both samples: [0.0125%-20nmAu-5CB(ori)] &[ 0.0125%-20nmAu-5CB(deg)] give us the good symmetricity and nonlinearity, similar to what we can observe under the frequency 10Hz. The value of the nonlinear coefficient (β) of the samples obtained from the fitting is shown in Table 4. Clearly, β is more at low concentrations.

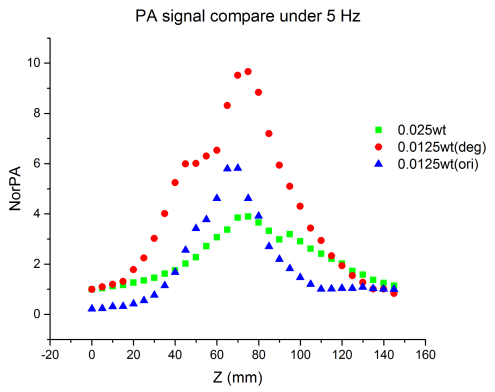
PA signal compare under 5 Hz
NorPA
Z (mm)
0.025wt
0.0125wt(deg)
0.0125wt(ori)

(a)

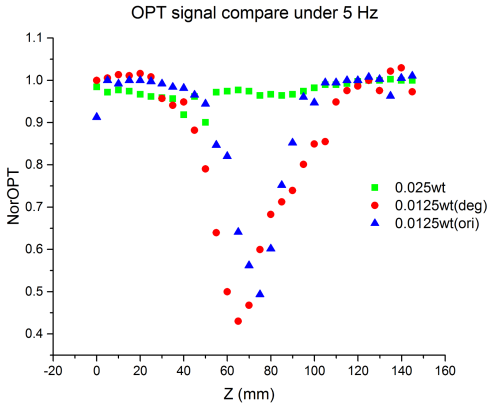
OPT signal compare under 5 Hz
NorOPT
Z (mm)
0.025wt
0.0125wt(deg)
0.0125wt(ori)

(b)

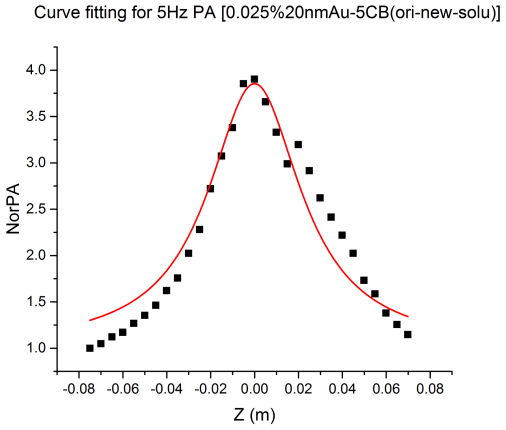
Curve fitting for 5Hz PA [0.025%20nmAu-5CB(ori-new-solu)]
NorPA
Z (m)

(c)

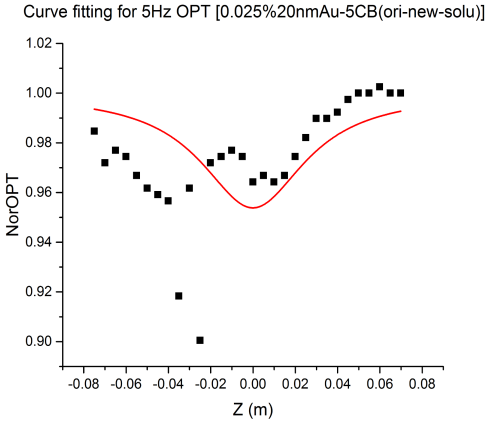
Curve fitting for 5Hz OPT [0.025%20nmAu-5CB(ori-new-solu)]
NorOPT
Z (m)

(d)

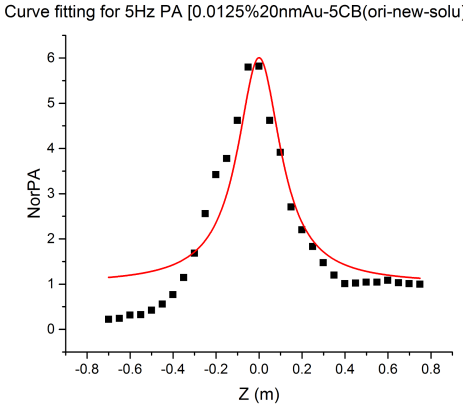
Curve fitting for 5Hz PA [0.0125%20nmAu-5CB(ori-new-solu)]
NorPA
Z (m)

(e)

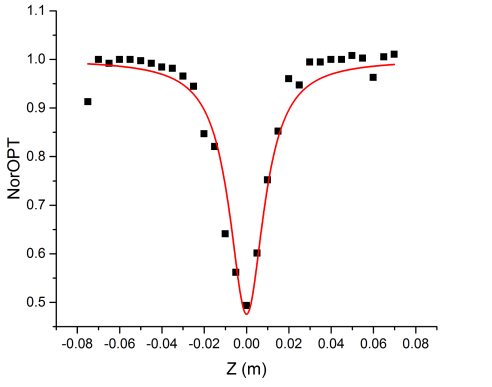
Curve fitting for 5Hz OPT [0.0125%20nmAu-5CB(ori-new-solu)]
NorOPT
Z (m)

(f)

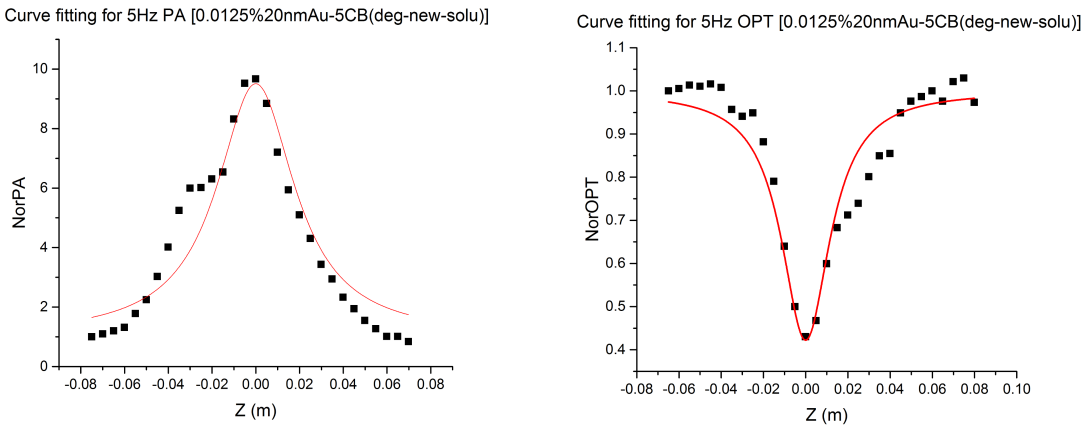


**(g)** **(h)**

Figure 19: Curve fitting and PA/OPT signal for 5 Hz laser pulse repetition frequency

Table 4 Values of nonlinear coefficient of different samples under 5Hz

| Samples | $\alpha(m^{-1})$ | $\beta$ (W/m) |
|---|---|---|
| 0.025%-20nmAu-5CB(ori) | 1470.978 | $2.96\times10^{-9}$ |
| 0.0125%-20nmAu-5CB(ori) | 2171.477 | $3.64\times10^{-8}$ |

### 3.3.3 Photoacoustic/optical signal and nonlinear coefficient β under 2 Hz

Decreasing the laser frequency from 5Hz to 2Hz shows a similar result. Good photoacoustic and optical z-scans were obtained at low concentrations, as shown in Figure 20a and Figure 20b. The optical signal for sample [0.025%-20nmAu-5CB (ori)], shown in Figure 20d, is not ideal, just like the result of what we obtained in the previous sections under 10 Hz and 5 Hz. This phenomenon may happen probably at specific concentrations; portions of the laser that passes through the sample have been reflected or scattered away, which leads to the reduction of light transmittance, resulting in such an optical signal pattern. Further study is needed to understand

this phenomenon comprehensively. Table 5 shows the value of the nonlinear coefficient (β) of samples under 2 Hz. Clearly, β is more at low concentrations.

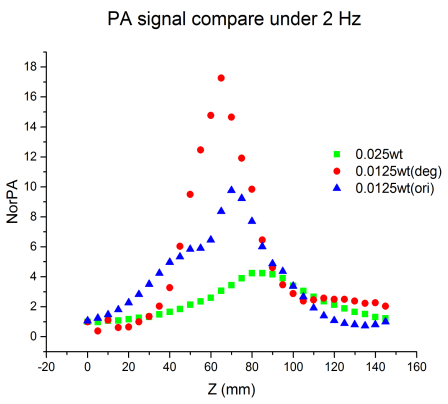


(a)

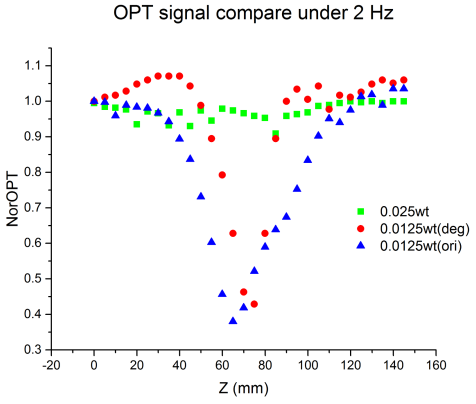


(b)

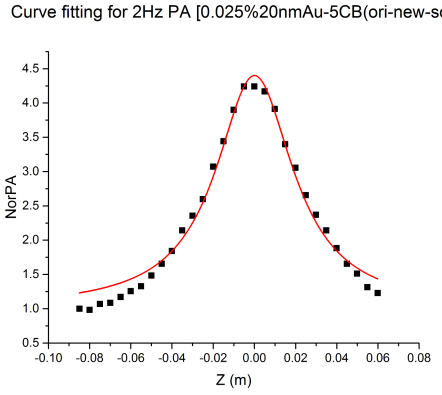


(c)

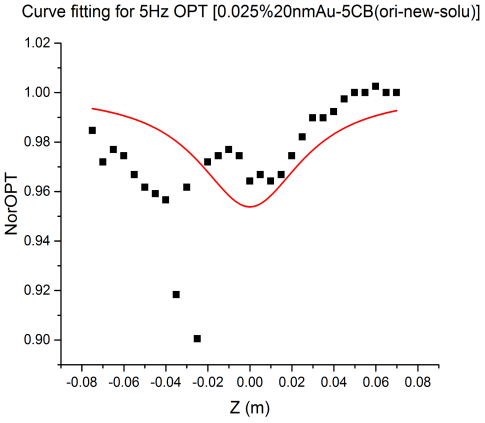


(d)

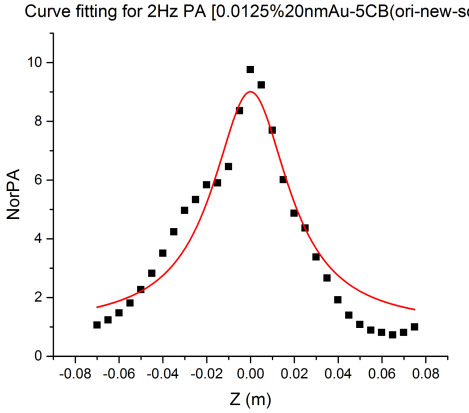


(e)

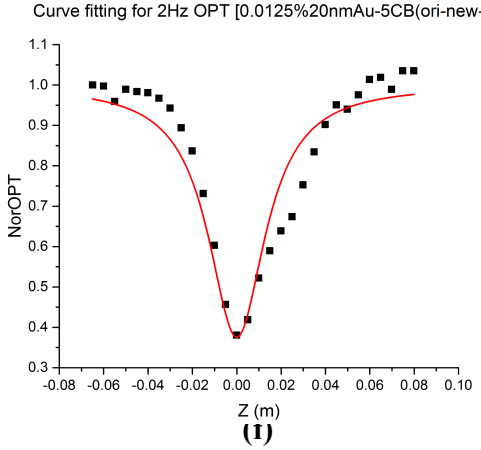


(f)

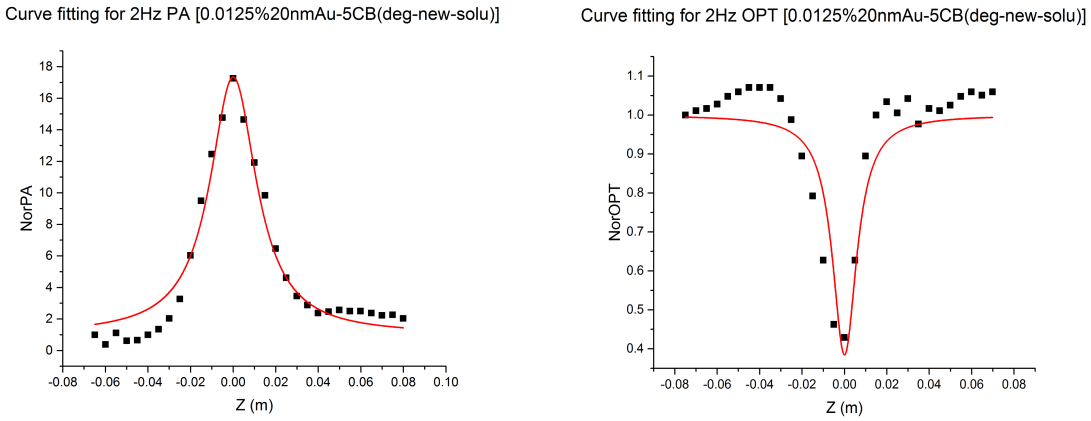


**(g)** **(h)**

Figure 20: Curve fitting and PA/OPT signal under 2 Hz

Table 5 Values of nonlinear coefficient of different samples under 2Hz

| Samples | α($m^{-1}$) | β (W/m) |
|---|---|---|
| 0.025%-20nmAu-5CB(ori) | 1470.978 | $3.15\times10^{-9}$ |
| 0.0125%-20nmAu-5CB(ori) | 2171.477 | $1.01\times10^{-8}$ |

### 3.4 Planar-oriented sample Vs. Planar-degenerated sample

In section 3.2, we observed that liquid crystal-based samples have better optical absorbance compared to water-based samples. Further, in section 3.3, for 0.0125 weight percent gold concentration at 2 Hz, 5 Hz, and 10 Hz, good PA and OPT signals were obtained, and the fitting curve showed good symmetricity and nonlinearity. Now the difference of nonlinear characteristics between planar-oriented and planar-degenerated liquid crystal cells are presented and discussed. As shown in Figure 21, although the PA and OPT signals for these two samples have similar patterns, comparing the signal plots for all frequencies carefully reveals that the

planar orientation (blue dots) shows better symmetricity than the planar-degenerated (red dots). The gold nanoparticles in planar-oriented cells tend to be more uniformly and evenly dispersed (Figure 16a). In comparison, the gold nanoparticles disperse freely inside the planar-degenerated cells and tend to aggregate together (Figure 16b). Table 6 shows the value of the nonlinear coefficient (β) of samples for all three laser repetition rates. Obviously, β is more at planar orientated liquid crystal cells. This result may be due to the different distribution of gold nanoparticles in the oriented/degenerated sample. Nanoparticles inside degenerated samples are freely distributed (Figure 7a). Therefore, this disorganized distribution may interfere with or reduce the SPR of gold nanoparticles. In the case of oriented samples, the gold nanoparticles are arranged neatly, which enhances SPR and, therefore, leads to better nonlinearity.

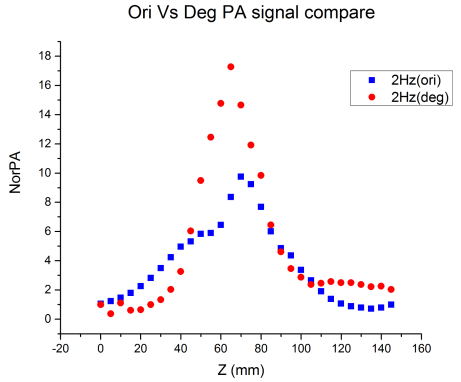


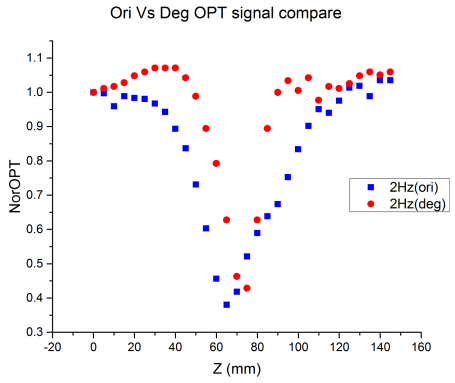


**(a)** **(b)**

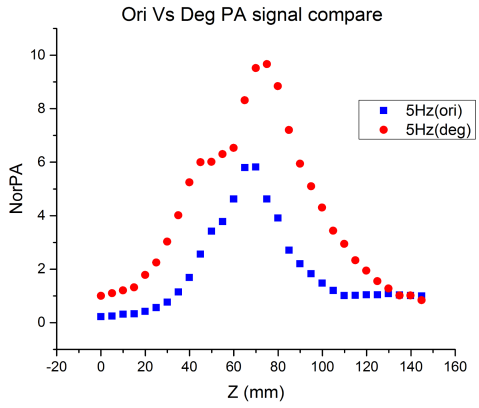


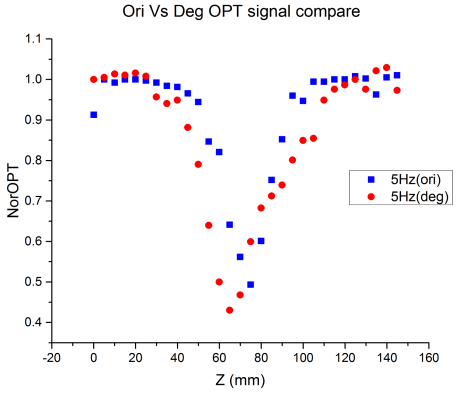

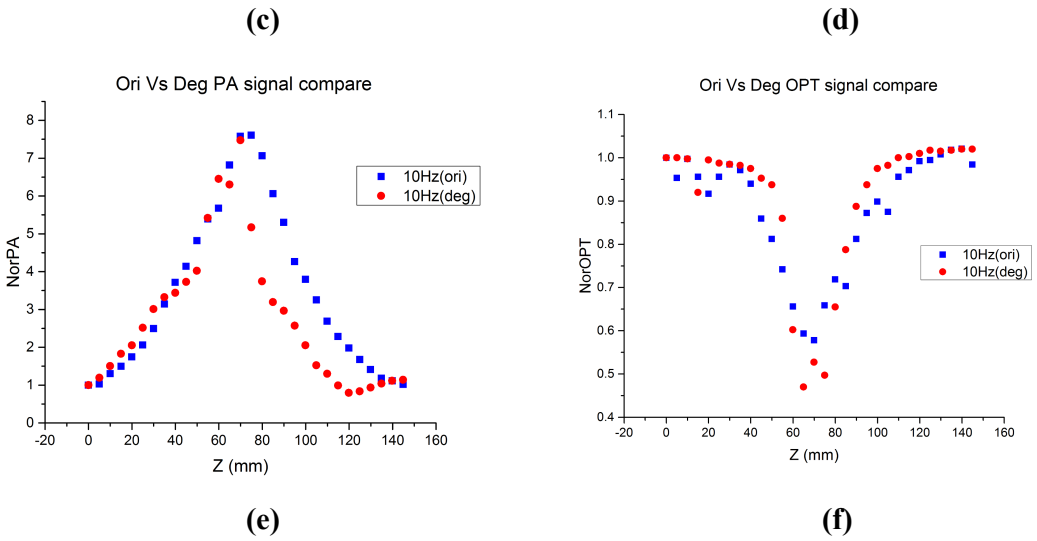


Figure 21: Planar-oriented sample Vs. Planar-degenerated sample

Table 6 Values of nonlinear coefficient of samples

| Laser repetition rate | Samples | $\alpha(m^{-1})$ | $\beta$ (W/m) |
|---|---|---|---|
| 10 Hz | 0.0125%-20nmAu-5CB(ori) | 2171.477 | $8.80\times10^{-9}$ |
| | 0.0125%-20nmAu-5CB(deg) | 1012.88 | $2.73\times10^{-9}$ |
| 5 Hz | 0.0125%-20nmAu-5CB(ori) | 2171.477 | $3.64\times10^{-8}$ |
| | 0.0125%-20nmAu-5CB(deg) | 1012.88 | $5.10\times10^{-9}$ |
| 2 Hz | 0.0125%-20nmAu-5CB(ori) | 2171.477 | $1.01\times10^{-8}$ |
| | 0.0125%-20nmAu-5CB(deg) | 1012.88 | $6.03\times10^{-9}$ |

# CHAPTER 4

## 4. CONCLUSION AND FURTHER STUDY

In conclusion, we studied the nonlinear optical properties of AuNps dispersed in nematic liquid crystals. Two types of liquid crystals cells were prepared – planar-oriented and degenerate. For the planar-oriented cells, gold nanoparticles concentration (by weight percentage) was varied. From the UV-Vis spectrum, linear absorption coefficient of samples [0.0125%-20nmAu-5CB(ori), 0.0125%-20nmAu-5CB(deg), 0.025%-20nmAu-5CB(ori) and 0.05%-20nmAu-5CB(ori)] were obtained. Nonlinear absorption coefficient (β) for samples were obtained using optical and photoacoustic Z-scan techniques where the laser repetition rate is varied as 2 Hz, 5 Hz, and 10 Hz. All samples show relatively good nonlinearity and nonlinear absorption coefficients. Among all samples, [0.0125%-20nmAu-5CB (ori)] shows the best PA/OPT signal plots and the desirable nonlinearity of Reverse Saturable Absorption. Further, the sample of low gold concentration made with planar-oriented 5CB liquid crystals shows the best PA/OPT signals and nonlinearity.

As the molecular and optical properties of liquid crystals are affected by temperature and applied electric field, how they will influence the nonlinearity of the gold nanoparticles dispersed in liquid crystals should be focused on in future research on this project.

REFERENCES


1. Nonlinear Optics 3rd Edition, Robert W. Boyd, 2008

2. Third order optical nonlinearities by Mansoor Sheik-Bahae, Michael P. Hasselbeck

3. Tomasz Borowski, "Photoacoustic in remote sensing," Proc. SPIE 11442,Radioelectronic Systems Conference 2019, 1144211 (11 February 2020); doi:10.1117/12.2565308

4. Nanotechnology in Medical Research, F.M. Mansfeld, M. Kavallaris, in Micro and Nanotechnology in Vaccine Development, 2017

5. In vivo imaging of graft-versus-host disease and graft-versus-leukemia, Dennis B. Leveson-Gower, Robert S. Negrin, 2013

6. Kruger RA. Photoacoustic ultrasound. Med Phys. 1994; 21:127–131

7. Oraevsky AA, Jacques SL, Esenaliev RO, Tittel FK. Time-resolved optoacoustic imaging in layered biological tissues. OSA Proc Advances in Optical Imaging and Photon Migration. 1994; 21:161–165.

8. Wang X, Pang Y, Ku G, Xie X, Stoica G, Wang LV. Noninvasive laser-induced photoacoustic tomography for structural and functional in vivo imaging of the brain. Nature Biotechnol. 2003; 21:803–806.

9. Beard Paul, 2011 Biomedical photoacoustic imaging interface Focus.1602–631

10. G.A. Ascoli, V. Tsytsarev, in Encyclopedia of the Neurological Sciences, 2014

11. Yao, J., & Wang, L. V. (2013). Photoacoustic Microscopy. *Laser & photonics reviews*, *7*(5), 10.1002/lpor.201200060. https://doi.org/10.1002/lpor.201200060

12. Surface plasmon resonance in gold nanoparticles: a review, Vincenzo Amendola et al 2017 J. Phys.: Condens. Matter **29** 203002

13. Interparticle Coupling Effect on the Surface Plasmon Resonance of Gold Nanoparticles: From Theory to Applications, Sujit Kumar Ghosh and Tarasankar Pal*Chem. Rev.* 2007, 107, 11, 4797–4862

14 Eric W. Van Stryland and Mansoor Sheik-Bahae "Z-scan technique for nonlinear materials characterization", Proc. SPIE 10291

15 Determining non-linear optical properties using the Z-scan technique, Pieter Neethling, 2005

16 R. Paschotta, article on 'nonlinear absorption' in the *Encyclopedia of Laser Physics and Technology*, 1. edition October 2008, Wiley-VCH, ISBN 978-3-527-40828-3

17 R. Paschotta, article on 'peak power' in the *Encyclopedia of Laser Physics and Technology*, 1. edition October 2008, Wiley-VCH, ISBN 978-3-527-40828-3

18 Rego JA, Harvey JA, MacKinnon AL, Gatdula E (January 2010). *Liquid Crystals*. **37** (1): 37–43. doi:10.1080/02678290903359291.

19 M. G. Tomilin , S. A. Povzun , A. F. Kurmashev , E. V. Gribanova & T. A.Efimova (2001) The application of nematic liquid crystals for objective microscopic diagnosis of cancer, Liquid Crystals Today, 10:2, 3-5, DOI: 10.1080/14645180110074819

20 Polarized Light Microscopy: Principles and Practice, CSHL Press, Cold Spring Harbor, NY, USA, 2011.

21 Mellqvist, J. and A. Rosén, DOAS for flue gas monitoring—II. Deviations from the Beer-Lambert law for the UV/visible absorption spectra of NO, NO2, SO2, and NH3. Journal of Quantitative Spectroscopy and Radiative Transfer, 1996. 56(2): p. 209-224.